The Journal of Chemical Physics

Extending the polarizable continuum model to effective *ab initio* pair potentials in multicomponent solutions: A test on calcium–water and calcium–ammonia potentials

Cite as: J. Chem. Phys. **116**, 5448 (2002); https://doi.org/10.1063/1.1453956
Submitted: 16 July 2001 • Accepted: 07 January 2002 • Published Online: 19 March 2002

F. M. Floris, José M. Martínez and J. Tomasi


View Online

Export Citation

ARTICLES YOU MAY BE INTERESTED IN

Preferential solvation of Ca^{2+} in aqueous solutions containing ammonia: A molecular dynamics study
The Journal of Chemical Physics **116**, 5460 (2002); https://doi.org/10.1063/1.1453957

The asymptotic region of the Kohn–Sham exchange potential in molecules
The Journal of Chemical Physics **116**, 5374 (2002); https://doi.org/10.1063/1.1453958

Density matrix variational theory: Application to the potential energy surfaces and strongly correlated systems
The Journal of Chemical Physics **116**, 5432 (2002); https://doi.org/10.1063/1.1453961

AIP Publishing

© 2002 American Institute of Physics.

Extending the polarizable continuum model to effective *ab initio* pair potentials in multicomponent solutions: A test on calcium–water and calcium–ammonia potentials

F. M. Floris, José M. Martínez,[a] and J. Tomasi
Dipartimento di Chimica e Chimica Industriale, Universitá di Pisa, Via Risorgimento 35, 56126 Pisa, Italy

(Received 16 July 2001; accepted 7 January 2002)

The use of the polarizable continuum model to develop *ab initio* effective pair potentials is extended to multicomponent solutions. The methodology takes into account nonadditivity effects on pair interactions computing wave functions perturbed by the solvent. Ca^{2+}–water and Ca^{2+}–ammonia potentials suitable for aqueous ammonia solutions are presented. These effective *ab initio* pair potentials present smaller binding energies with respect to strictly *ab initio* two-body potentials. The reduction is higher in Ca^{2+}–ammonia (28%) than in Ca^{2+}–water (22%) and brings to a small gap the difference between the binding energies of the two ligands with Ca^{2+} when solvent effects are considered. As a first test, metal-ligand clusters of different size and composition have been studied. The comparison with restricted Hartree–Fock *ab initio* calculations shows good agreement for the largest clusters considered. Results confirm that the presented methodology, based on the polarizable continuum model, describes in a proper way the interactions in the condensed phase, where the ion completes its coordination sphere. The cluster results also show that ammonia can displace water in the first ion coordination with a tendency to change the coordination number from 8 to 9 when the ion is fully surrounded by the former, the ninth ammonia molecule being positioned in an intermediate situation between the first and the second coordination shells. © *2002 American Institute of Physics.* [DOI: 10.1063/1.1453956]

I. INTRODUCTION

In the last two decades the number of published theoretical and experimental works in the field of solution chemistry has substantially increased, metal ion solvation being one of the subjects that has received much attention,[1–12] probably due to its relevance in a large part of chemical and physicochemical processes in nature, living organisms, and industrial technology.

From a theoretical point of view, there is an increasing interest in the combined application of quantum methodology with statistical simulations. In this sense the appearance of hybrid quantum mechanics/molecular mechanics methodologies[13] and *ab initio* molecular dynamics[14] has allowed one to get insight, at a very detailed level, into the solvation phenomenon of some metal ions.[15–25] However these techniques still suffer from some disadvantages, mainly the computational costs, which considerably limit the simulation times and the number of particles present in the simulation cell. This fact reduces the spectrum of accessible properties that can be studied using these methodologies. In this sense, classical statistical simulations,[26] Monte Carlo (MC) and molecular dynamics (MD), are still very useful and powerful tools that can provide valuable information. One of the key aspects for the successful outcome of the simulations is the use of proper interaction potentials, i.e., reliable results need realistic potentials.

In the case of metal ions, and particularly those multiply charged, the importance of so-called many-body effects is well known (see Refs. 27 and 28, and references therein), which must be taken into account to properly describe the ion–solvent interactions. The origin of these effects can be found in the induction phenomena caused by the ion electric field and in the charge transfer processes among the nearest solvent molecules and the metal ion. Polarizable models (see references in Ref. 28) become an interesting, and physically sound, way of including instantaneous polarization effects, usually by means of isotropic dipolar polarizability approaches. However, their use in statistical simulations is expensive because of the set of coupled linear equations to be solved. A reduction of costs is possible by the extended Lagrangian method in which charges are treated as additional dynamic variables.

Because of computer time savings, however, most of the classical simulations are performed under the assumption of pairwise additivity for the total interaction energy, so *effective* potentials which take into account these nonadditive effects must be used. Otherwise, misleading outcomes can be inferred from simulation results. This effectiveness can be introduced in the pair potentials using a set of experimental data, which is used as a source of information. Alternatively, one can explore quantum mechanically the potential energy surface (PES) of a cluster composed of one metal ion and a given number of solvent molecules as the source of energetic and structural information to develop ion–solvent intermolecular potentials.

This second strategy has become one of the most suc-

[a]On leave from Departamento de Química Física, Universidad de Sevilla 41012-Sevilla, Spain; electronic mail: josema@simulux.us.es

 © 2002 American Institute of Physics

cessful ones to overcome the problem of using pair potentials to study metal ion solvation by means of classical simulations (see Ref. 28, and references therein). If the cluster, whose PES is studied, contains N solvent molecules, contributions up to $N+1$ terms are explicitly included in the ion–solvent potential. This supermolecule approach is, in some cases, demanding in terms of computational times because of the size of the cluster.[29–31] One has to keep in mind that, in most of the cases, several hundreds of calculations are necessary to properly consider the different representative arrangements, although specific strategies can considerably reduce this figure.[32–34]

An alternative way of including the effects of the surrounding medium is to consider solvent effects in an implicit way. This type of methodology has already been successfully applied by some of us[35–37] with the help of the polarizable continuum model (PCM),[38,39] which describes the solvent as a dielectric continuum characterized by a permittivity ϵ. In this way, many-body effects are included in the ion–solvent potential but keeping at the same time the computational convenience and simplicity of two-body functions in the development process.

The methodology has allowed the development and application on MD simulations of effective potentials for a series of cations in water.[35–37] The final validation of this type of theory-based potentials is done on the basis of the comparison between the simulation results and the available experimental information for the simulated system. Good agreement has been observed for structural[28,35,36,40,41] and thermodynamic[37,41] properties for a certain number of cations with charge $+1$, $+2$, and $+3$.

Interesting enough, and by far quite less studied, are those complex situations where more than one solvent is present in the ionic solution. Particularly, aqueous solutions containing small proportions of other potential ligands constitute the most common situation in the biological media. In addition to this biochemical interest, the development of methodologies able to treat these complex media at the same level as that reached in the case of pure aqueous solutions is a theoretical challenge, and steps in this direction must be given to properly understand the metal complexation phenomena with different species in solution.

The work presented here, motivated by this fact, supposes an extension of the previously applied strategy[35–37] to develop ion–water *ab initio* interaction potentials on the basis of the PCM methodology to include solvent effects. The study will be performed using Ca^{2+} as the metal ion, surely one of the most studied ions because of its prominent biological role.[42,43] In addition to water, ammonia is chosen as second potential ligand for two main reasons. On one hand, because of its simplicity, it supposes a natural choice for extending the methodology in a stepwise fashion. On the other hand, its behavior, from the point of view of the metal–ligand interaction, is rather similar to that of water.

In this work a preliminary test of the newly developed potentials is done on the basis of cluster computations. Their application in MD simulations of aqueous ammonia solutions containing the Ca^{2+} is presented elsewhere.[44]

II. POTENTIAL DEVELOPMENT

A. Effective pair potentials in the context of the polarizable continuum model

Details about the use of the PCM to develop effective *ab initio* pair potentials is described elsewhere.[28,35,37] A short overview is presented here to facilitate the understanding of the extension done in this work.

The procedure is based on the use of the polarizable continuum model for the evaluation of the solvent influence on specific interactions. The solvent is modeled by an isotropic dielectric medium which surrounds the solute, for which an appropriate cavity is defined. The electrostatic potential generated by the solute charge distribution induces a polarization charge σ on the cavity surface because of the solvent polarization. This polarization of the solvent also induces a solute charge redistribution which is taken into account by means of a modified Hamiltonian:

$$\hat{H}=\hat{H}^{(0)}+\hat{V}_{\sigma}, \tag{1}$$

where $\hat{H}^{(0)}$ is the Hamiltonian for the isolated solute, $\hat{V}_{\sigma}$ the monoelectronic operator associated with the electrostatic potential V_{σ} generated by the charge distribution σ present in the surface of a cavity that contains the solute. Considering two generic fragments, A and B, the nonadditive effects are then considered through the modification of the interaction potential of the $A\cdots B$ pair. According to this idea, the effective interaction potential U_{AB} is defined as

$$U_{AB}=\langle\Psi|\hat{H}^{(0)}|\Psi\rangle_{AB}-\langle\Psi|\hat{H}^{(0)}|\Psi\rangle_{A}-\langle\Psi|\hat{H}^{(0)}|\Psi\rangle_{B}, \tag{2}$$

where the Ψ's are eigenfunctions of the $\hat{H}$ operator, i.e., perturbed by the solvent, and correspond to the complex AB and to the isolated species embedded in the solvent. Equation (2) gives a definition for U_{AB} in which the interaction energies of A, B, and AB with the dielectric continuum has been removed, yielding only the direct interaction between A and B, modified in the dielectric medium through the changes of their wave functions. This is necessary because during the statistical simulations, the continuum is replaced by explicit solvent molecules which interact with the solute fragments according to their respective interaction potentials.

The difference between Ψ and the wave function of the isolated molecule, Ψ^0, depends on the dielectric constant of the solvent and the shape of the cavity. We notice that when necessary, as in many geometrical configurations considered in this work, PCM introduces separated cavities. The cavity is built on the base of a set of interlocking spheres centered on atomic nuclei. The variation of the radii (r_i) of the spheres will then affect the computed effective potential. This dependence is precisely the one exploited to tune the additivity of the effective pair potential. In the case of metal aqueous solutions, for O and H atoms, the standard radii[45] have been assumed, $r_{\mathrm{O}}=1.68$ Å and $r_{\mathrm{H}}=1.44$ Å. Instead, the radius of the sphere centered on the cation (r_M) has been fixed in a way that the three-body potential for the complex WMW' embedded in the dielectric can be decomposed into the sum of two-body effective potentials,

TABLE I. Interaction energies and optimized geometries of the $[CaL]^{2+}$ complexes.

Basis sets ref.	Level	$[CaNH_3]^{2+}$		$[CaH_2O]^{2+}$	
		R_{Ca-N} (Å)	E_{int} (kcal/mol)	R_{Ca-O} (Å)	E_{int} (kcal/mol)
36[a]	RHF	2.52	−57.5	2.36	−53.2
46[b]	QCISD	2.42	−61.0	2.27	−53.4
This work[c]	RHF	2.43	−60.8	2.29	−54.3

[a]ECP calculation for Ca^{2+} with $1s$ and $2sp$ electrons in core (Ref. 60) and six Cartesian d functions from Ortega-Blake *et al.* (Ref. 61). For O and H atoms, Huzinaga–Dunning $[3s2p/2s]$ basis sets increased with a d function ($\zeta=0.85$) for (Refs. 36 and 37).
[b]6-31G^{**}.
[c]6-311+G^{**}.

$$U_{WMW'}(r_M)=\langle\Psi|\hat{H}^0|\Psi\rangle_{WMW'}-\langle\Psi|\hat{H}^0|\Psi\rangle_M-\langle\Psi|\hat{H}^0|\Psi\rangle_W-\langle\Psi|\hat{H}^0|\Psi\rangle_{W'}=U_{MW}(r_M)+U_{MW'}(r_M)+U_{WW'} \quad (3)$$

for a relevant geometry of the trimer. Water–water interactions are treated by means of a pair potential, that to be used in the simulations. In this sense, the modifications on the solvent–solvent interactions originated by the presence of the ion will be included in the ion–water potential as well. Once the value of r_M obeying Eq. (3) is found, a scanning of the $M\cdots W$ potential energy surface in the continuum is performed, using that value to define the sphere around the metal ion. Effective interaction energies are then extracted according to Eq. (2).

The extension of this methodology to the case in which a second potential ligand is considered, ammonia (A) in our case, implies, in the more general case, the consideration of three equations similar to Eq. (3), which come from the possibilities one can find in the first coordination shell of the ion:

$$U_{WMW'}(r_M)=U_{MW'}(r_M)+U_{MW'}(r_M)+U_{WW'}, \quad (4a)$$

$$U_{WMA}(r_M)=U_{MW}(r_M)+U_{MA}(r_M)+U_{WA}, \quad (4b)$$

$$U_{AMA'}(r_M)=U_{MA}(r_M)+U_{MA'}(r_M)+U_{AA'}. \quad (4c)$$

If we maintain the same level of simplicity as that previously applied, we find three independent equations and one variable, r_M, to fulfill them. For each equation a solution comes out, so, in principle, three different solutions, each one fulfilling one equation, are possible. However, this raises the difficulty of the ion radius that should be used when performing the scanning of $M\cdots W$ and $M\cdots A$ potential energy surfaces, because two solutions come out for each ligand [4(a) and 4(b) for water, and 4(b) and 4(c) for ammonia]. In order to solve this problem maintaining an internal consistency (just one radius for each atom) a compromise between the solutions obtained from the three previous equalities is applied. To achieve that, a combination among the three radii is performed in order to minimize the total error coming from the difference between the three body energies [left-hand side of Eq. (4)] and the value obtained assuming pairwise additivity (right-hand side) for the three equations simultaneously. Obviously this way of working introduces some inaccuracies in the method, compared to the former case (MWW') in which Eq. (3) was strictly verified. However, as will be shown in Sec. II B, solutions to the three equations are close enough to guarantee a final result in which the percentage of error introduced by this fact is below the approximations inherent to the way nonadditive effects are taken into account. An alternative procedure in which equalities of Eq. (4) are strictly verified implies the use of two other parameters, i.e., radii, to fulfill the equations. However, a well tested set of radii, in the context of the PCM methodology, are available nowadays for atoms like C, N, O, or H, and their accuracy in reproducing structural and energetic aspects of the solvation process of a large set of compounds have been proven, (see e.g., Ref. 45). In this sense, the approach followed here maintains that level of accuracy achieved for the ligands used.

B. $Ca^{2+}-H_2O$ and $Ca^{2+}-NH_3$ effective interaction potentials

Based on the existence of a $Ca^{2+}-H_2O$ interaction potential previously developed with the described methodology, the first idea was to obtain a new one for the $Ca^{2+}-NH_3$ interaction using the same level of computation as that used in Ref. 36 for the $Ca^{2+}-H_2O$ one, i.e., restricted Hartree–Fock (RHF) computations using an effective core potential for calcium ion and basis sets of double zeta quality on water plus a d function on the oxygen. However, using the optimized geometry of ML^{2+} clusters as test systems, the difference in the interaction energy, computed in vacuum, for the $[Ca-H_2O]^{2+}$ and $[Ca-NH_3]^{2+}$ systems was only 4.3 kcal/mol (Table I). A very recent study,[46] performed with a high level *ab initio* method (QCSID/6-311G^{**}), estimates this difference in 7.6 kcal/mol. Because this interaction energy difference will be, presumably, one of the factors dominating the differences in ion complexation showed by the two ligands, we think is worth to develop both ion–ligand potentials using a level of computation that doesnot underestimate this energy differences as much.

More than 400 $[ML]^{2+}$ computations will be needed for each ligand, so such a high (and time demanding) level of computations cannot be afforded. In this sense, Kerdcharoen and Hannonguba[47] have shown the marginal effect that electron correlation, at the MP2/6-31G^{**} level, has on the interaction energies for a set of calcium–ammonia clusters. Moreover, the metal–ligand interaction energy for the high-

TABLE II. Weighted average values of U_3^0 and the corresponding ligand–metal—ligand angles.[a]

Ligand pair	U_3^0 (kcal/mol)	$\angle L_1ML_2$ (deg)
Water–water	5.1	80.8
Water–ammonia	5.9	80.1
Ammonia–ammonia	7.4	80.3

[a]Relative ligand–ligand orientations are shown in Fig. 1.

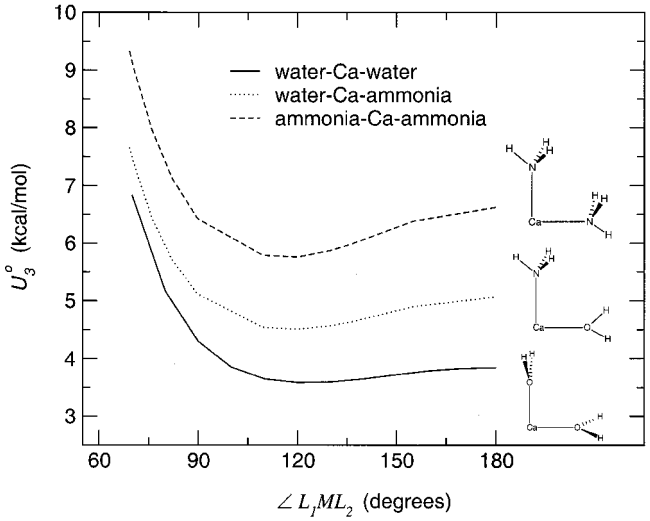

FIG. 1. Evolution of the three-body term as a function of the ligand–metal–ligand angle. Insets show relative ligand–ligand orientations.

est cluster considered, $[Ca(NH_3)_6]^{2+}$, differs only in 1% when RHF and second-order Møller-Plesset (MP2) levels of calculation are compared. In the case of water clusters, $[Ca(H_2O)_n]^{2+}$ with $n=8$, 9 and basis sets of triple-zeta quality, the effect of the electronic correlation computed[36] at the MP2 level is small as well (4%–5%).

Those results are not surprising. In fact, in this type of system, dispersion interactions, derived from the mutual instantaneous polarization, are less important than polarization effects, because of the low polarizability of the cation. Taking into account these results and those found in Ref. 48 regarding the use of diffuse functions on solvent molecules to afford energetic aspects, all the *ab initio* metal–ligand computations done in this work have been performed at the RHF/6-311+G^{**} level using the GAUSSIAN99 package.[49] PCM computations were performed following the IEF: Integral Equation Formalism implementation.[50,51]

Table I shows the cation–ligand interaction energies and the metal–oxygen and metal–nitrogen distances for the gas phase fully optimized structures, obtained with that level of calculation. For the sake of clearness, results from previous works are shown as well. We notice that for the calcium–water system, the RHF interaction energy computed using ECP for Ca^{2+} [36] is in very good agreement with the high level *ab initio* calculation of Ref. 46. The disagreement in the energy difference between $[Ca(H_2O)]^{2+}$ and $[Ca(NH_3)]^{2+}$ comes in fact from the underestimation in the interaction energy of the $[Ca(NH_3)]^{2+}$ system. However, for cation–water interactions, it has been found that the effect of full electron calculations and the improving of basis sets (up to TZP) is generally well compensated with the correlation effects.[37] It can be seen that the full electron calculations at RHF/6-311+G^{**} yield energies and structures closer to the ones obtained with the reference computations,[46] differences being acceptable considering the scanning to be performed in the potential energy surfaces.

As described in Sec. II A, the value of the Ca^{2+} radius is based on the pairwise additivity constraints of Eq. (4). In order to evaluate such equalities, relevant geometries should be used. Metal–ligand distances were fixed to values slightly longer (2.4 and 2.5 Å for R_{Ca-O} and R_{Ca-N}, respectively) than those of the potential minima for each dimer, due to the enlargement observed when the number of molecules in the first coordination shell increases.

A second important parameter is the ligand–metal–ligand angle ($\angle L_1ML_2$). Nonadditive effects are strongly dependent on this parameter as can be observed in Fig. 1 where U_3^0, defined as the difference between the total interaction energy for a given trimer and the sum of all pair interaction energies, is plotted. The superscript 0 indicates that all the *ab initio* interaction energies are computed in vacuum. Experimental water[52] and ammonia[53] geometries were used while the relative ligand–ligand orientation was optimized in each case to minimize repulsions. Obviously, if nonaddictive effects were not present, U_3^0 would be equal to zero.

Previously,[35–37] a weighted average of U_3^0 had been computed on the basis of the recurrence of the angles defining tetrahedral, octahedral, and cubic complexes. The value of U_3^0 in this way computed, was then interpolated in the corresponding representation, analogous to those of Fig. 1, to extract the value of $\angle L_1ML_2$ that corresponds to this average nonadditivity. That angle was the one used in the evaluation of expression (3) in order to obtain the value of r_M.

In this work, a slightly different approach has been followed. First, the geometrical structures used to compute the weighted average value of U_3^0 are based on the MD results of Ref. 36 where the most representative structures were first coordination shells with eight and nine water molecules. In this sense, the regular geometrical figures used are the square antiprism and the tricapped trigonal prism. Second, a new factor comes out, that is the possibility of three different pairs of ligands. It is clear from Fig. 1 that, for a given value of $\angle L_1ML_2$, each pair of ligands yields a different value of U_3^0. To take into account this new degree of freedom, all the stoichiometries were considered, i.e., from CaW_nA_0 to CaW_0A_n (with $n=8,9$), and for each of these complexes, all the different distributions of the ligands were taken into account. In this way, for the three different pairs, weighted average values of U_3^0 were obtained. Table II collects these results and the corresponding $\angle L_1ML_2$ values for each case. The proximity of the three angles allows us to average them, resulting in a final $\angle L_1ML_2$ of 80.4°. With this result, the search of $r_{Ca^{2+}}$ is then performed using equalities present in Eq. (4).

Figure 2 shows the left- and right-hand sides of those equalities as functions of the sphere radius of the cation. The

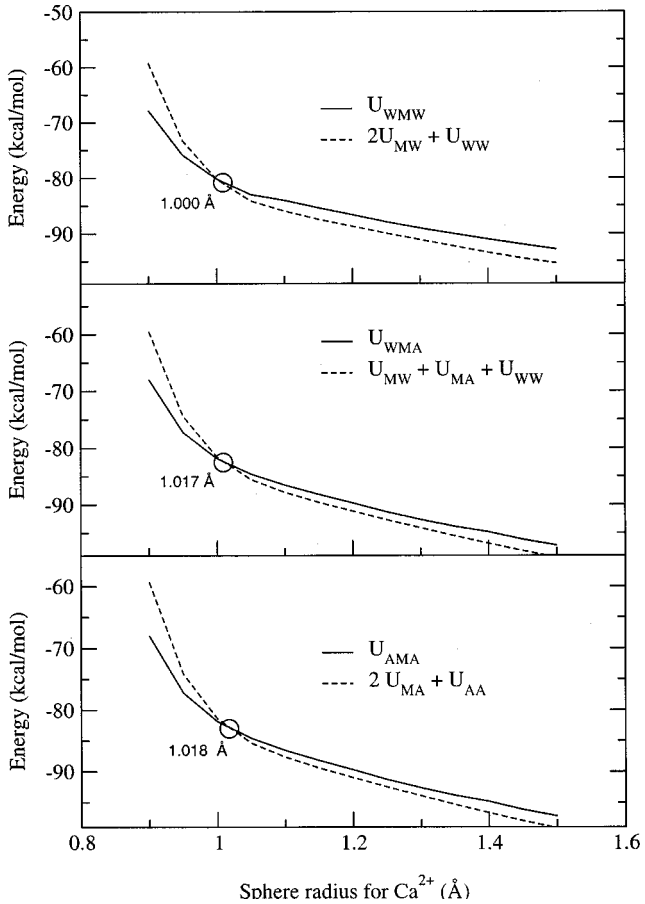

FIG. 2. Effective interaction energies as a function of the sphere radius of the cation. Full lines correspond to PCM computations with two solvent molecules and dashed lines to the sum of two-body contributions.

crossing points, i.e., those where equalities are strictly verified in each case, are 1.000, 1.017, and 1.018 Å. The final value to be used in the development of the calcium–water and calcium–ammonia interaction potentials is chosen as a linear combination of these three values in such a way that the final error summed over the three equations is minimized. After attempting several combinations, the simple arithmetic average, 1.012 Å, reports a value of 0.0 kcal/mol, coming from a compensation of errors among the three equations; the largest discrepancy being just 0.3 kcal/mol for the water–Ca^{2+}–ammonia trimer.

Once the cation radius is defined, a sampling of the $Ca^{2+}-H_2O$ and $Ca^{2+}-NH_3$ potential energy surfaces in solution is performed, maintaining rigid the water and ammonia geometries. Because the final aim is the simulation of aqueous solutions containing small amounts of ammonia, the dielectric constant used in these computations was that of water solvent. Calcium–water surface sampling was composed of 428 points while that of the calcium–ammonia contained 486. In both cases, all points were generated by means of Ca–O and Ca–N distance series in which different metal–ligand orientations were considered. Minima were located for C_{2v} and C_{3v} geometries with Ca–O and Ca–N distances of 2.38 and 2.44 Å, respectively. These equilibrium distances are about 0.1 Å longer than the corresponding obtained in vacuum. In addition, interaction energies were reduced by 22% (from −54.6 to −42.8 kcal/mol) in the case of water and by 28% (from −60.7 to −43.6 kcal/mol) in the case of ammonia. In this way, the difference in the effective interaction energies of both ligands with Ca^{2+} in aqueous solution, computed at the minimum of each potential energy surface, is only by about 1 kcal/mol. Using Eq. (2), effective interaction energies were extracted and fitted to an analytical function of site–site type:

$$E_{\text{int}}(ML) = \sum_{i}^{L\ \text{sites}} \frac{q_M q_i}{R_{Mi}} + \frac{C_4^{Mi}}{R_{Mi}^4} + \frac{C_6^{Mi}}{R_{Mi}^6} + \frac{C_8^{Mi}}{R_{Mi}^8} + \frac{C_{12}^{Mi}}{R_{Mi}^{12}} + A_{Mi} e^{-B_{Mi} R_{Mi}}, \tag{5}$$

where R_{Mi} is the distance between the calcium atom and the site i of the ligand L, and A, B, and C the fitted parameters. Fitting was performed using the geometries and charges of the solvent models to be used in the simulations, SPC/E for water[54] and OPLS for ammonia.[55] In addition to the atomic positions, an additional uncharged and massless site was defined in both ligands when computing ion–L interactions. This new site (X), whose final position was optimized as well, was located on the C_{2v} and C_{3v} axes of water ($R_{\text{O–X}} = 0.3$ Å) and ammonia ($R_{\text{N–X}} = 0.4$ Å) molecules, respectively, on the same side of hydrogen atoms. Parameters for both potentials are reported in Table III. The quality of both fits can be observed in Fig. 3 where the fitted energies are plotted against the corresponding *ab initio* ones. Standard deviations of 0.33 and 0.59 kcal/mol were obtained for Ca^{2+}–water and Ca^{2+}–ammonia potentials, respectively. These figures are roughly divided by two when just attractive energy points are considered.

III. A FIRST APPLICATION: CLUSTER COMPUTATIONS

Although the final aim is the use of the new potentials in statistical simulations of aqueous ammonia solutions, a preliminary test of them has been performed by means of cluster

TABLE III. Parameters of the Ca^{2+}–water and Ca^{2+}–ammonia effective potentials. Units consistent with interaction energies in kcal/mol and distances in Å.

	Site	C_4	C_6	C_8	C_{12}	A	B	q
Ca–H_2O	O	26.1392	2624.77	4 879.63	−16 949.8	29.3765	0.4	−0.8476
	H	1267.66	−7082.91	13 044.8	−13 073.5	20.2808	0.4	0.4238
		−1398.41	4653.32	−947.297	−27 150.0	−123.148	0.5	0.0
Ca–NH_3	N	−2929.79	18 610.1	−15 043.4	−12 244.3	−42.1194	0.32	−1.02
	H	1845.95	−12 714.8	28 965.5	−42 683.0	69.7683	0.4	0.34
		−62.2891	12 599.6	−69 473.0	210 265.0	−277.758	0.5	0.0

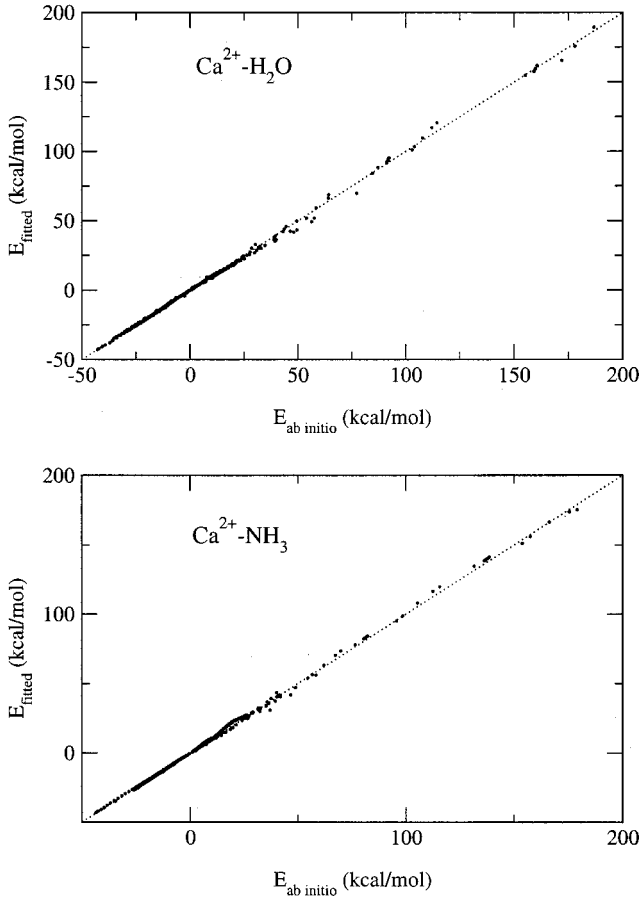

FIG. 3. Correlation between the effective two-body and *ab initio* interaction energies for the calcium–water and calcium–ammonia dimers.

computations. First, by comparison with the analog quantum calculations, the performance of the potentials can be tested, at least for small systems. Second, because of the low computational price, many different cluster compositions can be studied, allowing one to follow the environmental changes happening in the neighborhood of the ion when solvent composition changes.

In addition to calcium–water and calcium–ammonia clusters, clusters containing both ligands have also been studied. Due to the large number of possible mixed clusters, $[Ca(H_2O)_n(NH_3)_m]^{2+}$, we restrict our interest to those fulfilling $n+m=8$ with $n=m=4$. This choice allows us to evaluate the performances of $Ca^{2+}-H_2O$ and $Ca^{2+}-NH_3$ potentials in those situations where nonadditive water–calcium–ammonia terms are very important. The coordination number 8 for calcium is one of the favorites in aqueous solutions,[8] while an equal composition of both ligands maximizes the number of three-body water–calcium–ammonia interactions.

Clusters were minimized using DLPOLY[56] code and the aforementioned potentials. For the analogous ones obtained at a quantum chemical level, geometry optimizations were performed at the same level used for potential development (RHF/6-311+G^{**}), keeping frozen internal water and ammonia geometries and equal to those used in the calculations with the effective pair potentials (EPP).

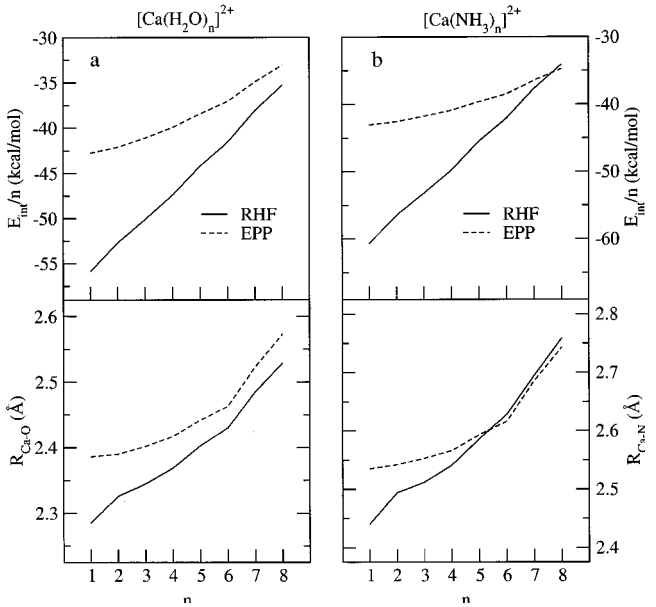

FIG. 4. Evolution of the interaction energy and mean Ca–O and Ca–N distances as a function of the number of water (left) and ammonia molecules (right). Solid lines correspond to RHF/6-311+G^{**} computations, and dashed ones to effective pair potentials calculations.

A. Calcium–water clusters

Clusters containing up to eight water molecules were studied at both levels. In both types of computations, minima with all the waters in the first coordination shell of Ca^{2+} were observed, as previously found in other works concerning quantum chemical studies.[48,57] A closer inspection of the cluster geometries reveals that in all cases the coordination polyhedra found in the RHF and EPP optimized structures are the same.

Figure 4(a) shows the evolution of the total interaction energy (normalized by the number of water molecules) and the Ca–O average distance as a function of the number of water molecules for both types of calculations. The expected behavior is observed in both cases: many-body effects increase the Ca–O distance and decrease the interaction energy.

Interestingly, the results obtained by means of the effective potentials are closer to the quantum chemical ones for the largest clusters, i.e., those in which a complete first coordination shell can be identified. Differences between RHF and EPP curves are continuously decreased as long as n increases. For $n=8$, they are only 6% and 2% for the interaction energy and the calcium–oxygen distance, respectively. This behavior reflects how the methodology we have followed, works properly in cases where the neighborhood of the ion resembles as much as possible that of the condensed medium, i.e., a metal ion completely solvated, as is the case of the clusters with largest values of n. This is due to the way many-body effects have been included.

It is worth pointing out that this behavior is just the opposite to that found using *ab initio* (strictly) two-body potentials: the larger the number of molecules coordinating the metal ion, the larger the differences between the *ab initio* and pair potential results are found (see, for instance, Ref. 47).

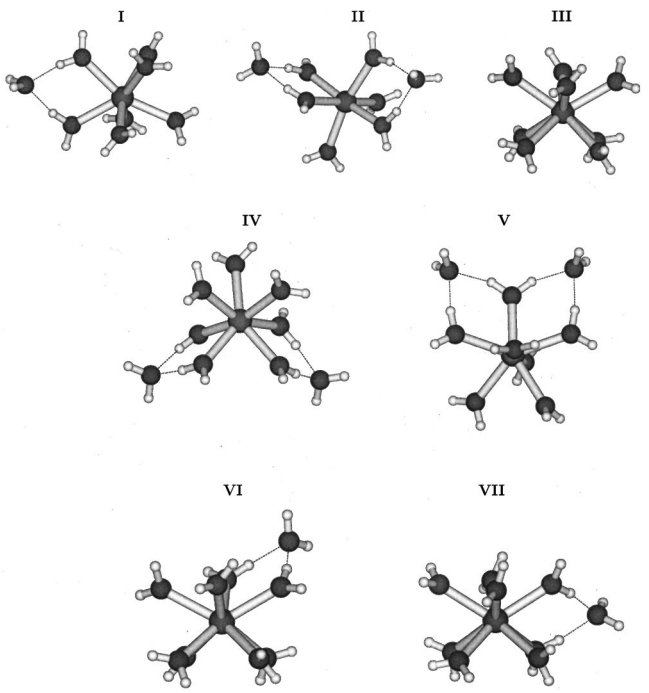

FIG. 5. Minima obtained for water clusters containing eight and nine solvent molecules. The corresponding interaction energies are shown in Table IV. Atom coordinates are available as electronic data files (Ref. 62).

Calculations at the MP2 level[57] on clusters with $n=8$ have shown that a change in the number of water molecules directly bonded to the calcium ion is allowed with a minimum amount of net energy gain or loss. EPP optimizations of $[Ca(H_2O)_6(H_2O)_2]^{2+}$, $[Ca(H_2O)_7(H_2O)]^{2+}$, and $[Ca(H_2O)_8]^{2+}$ clusters (structures II, I, and III in Fig. 5) yield interaction energies whose differences define a narrow range, 1.1 kcal/mol, in agreement with the results obtained by Katz *et al.*,[57] 1.5 kcal/mol. In our EPP calculations the octa-coordinate structure (III) is less stable than the hexa- and hepta-coordinate ones, the latter being almost degenerate. With the narrow energy ranges and the dependence of quantum chemical calculations on basis sets, the difference found in the stability sequence between the EPP results and those of Katz*et al.*[57] seems not very significant.

Optimization of clusters with nine water molecules at EPP showed no minima in which all molecules were accommodated in the first coordination sphere. However, two different minima were identified for geometries of the type $[Ca(H_2O)_7(H_2O)_2]^{2+}$ (IV and V in Fig. 5) and $[Ca(H_2O)_8(H_2O)]^{2+}$ (VI and VII), the former ones being preferred by ~2 kcal/mol.

Octa-hydrated complexes in a square antiprism geometry had also been found in MD simulations of infinitely dilute solutions of Ca^{2+}.[37,58] We notice that structures VI and VII resemble a square antiprism with the ninth water making hydrogen bonds with two waters belonging to the same (VI) or different (VII) square faces of the polyhedrum.

Finally, EPP optimized structures have been used to compare the interaction energies at effective pair potential and *ab initio* RHF levels (see Table IV). This comparison allows us to make a more precise evaluation of the differences between the EPP and RHF results. Differences between the two kinds of calculations range from a minimum of ~4% (structure II) up to 10.5% (structure VII). EPP interaction energies are always overestimated, i.e., the nonadditivity is slightly underestimated, as already found in Ref. 37 for effective pair potentials based on PCM and SPC/E water. However, in that study, geometries were optimized at each level. In particular, for calcium complexes with $n=8$, 9 nonadditive effects were slightly overestimated, in agreement with what we have observed in structure III. Nonethe-

TABLE IV. Effective pair potentials interaction energies, ΔE^{EPP}, *ab initio* RHF interaction energies, $\Delta E^{ab\ initio}$, computed on EPP optimized clusters and average first coordination shell Ca–O and Ca–N distances, $\overline{R}_{Ca-X}$. Units in kcal/mol and Å.

Cluster	ΔE^{EPP}	$\Delta E^{ab\ initio}$ [a]	$\overline{R}_{Ca-X}$
$[Ca(H_2O)_6(H_2O)_2]^{2+}$(II)	−265.5	−255.0	2.45±0.02
$[Ca(H_2O)_7(H_2O)]^{2+}$(I)	−265.8	−251.2	2.52±0.02
$[Ca(H_2O)_8]^{2+}$(III)	−264.7	−247.7 (−282.4)	2.573±0.0
$[Ca(H_2O)_7(H_2O)_2]^{2+}$(IV)	−286.1	−263.9	2.51±0.02
$[Ca(H_2O)_7(H_2O)_2]^{2+}$(V)	−285.4	−264.9	2.51±0.03
$[Ca(H_2O)_8(H_2O)]^{2+}$(VI)	−284.4	−259.5	2.57±0.02
$[Ca(H_2O)_8(H_2O)]^{2+}$(VII)	−284.0	−256.2	2.57±0.02
$[Ca(NH_3)_8]_{2+}$	−277.6	−271.0 (−272.8)	2.743±0.0
$[Ca(NH_3)_8(NH_3)]^{2+}$(I)	−294.4	−282.9	2.74±0.03
$[Ca(NH_3)_8(NH_3)]^{2+}$(II)	−294.1	−277.5	2.74±0.04
$[Ca(NH_3)_8(NH_3)_2]^{2+}$(III)	−310.6	−290.8	2.73±0.02
$[Ca(NH_3)_8(NH_3)_2]^{2+}$(IV)	−310.4	−290.5	2.73±0.04
$[Ca(NH_3)_8(NH_3)_2]^{2+}$(V)	−310.2	−286.1	2.73±0.05
$[Ca(NH_3)_8(NH_3)_2]^{2+}$(VI)	−309.7	−285.0	2.73±0.02
$[Ca(H_2O)_4(NH_3)_4]^{2+}$(I)	−271.6	−259.6 (−278.7)	
$[Ca(H_2O)_4(NH_3)_4]^{2+}$(II)	−270.8	−257.5 (−276.1)	
$[Ca(H_2O)_4(NH_3)_4]^{2+}$(III)	−271.3	−259.1 (−278.3)	
$[Ca(H_2O)_4(NH_3)_4]^{2+}$(IV)	−271.1	−257.8 (−276.5)	

[a]Values in parentheses refer to RHF optimized structures.

less, differences between RHF and EPP interaction energies depend on the structures used. When the *ab initio* optimized geometry of $[Ca(H_2O)_8]^{2+}$ is used, the geometrical relaxation decreases ΔE leading to a lower value than that computed at EPP level.

Comparing clusters with the same number of waters, differences between EPP and RHF results are inversely proportional to the average Ca–O distance for waters in the first coordination shell (see Table IV). The minimum error is observed in structure II, which interestingly presents a value for the Ca–O distance very close to 2.4 Å, the fixed value in the selected geometries used to fulfill Eq. 4(a). The other important parameter fixed in the application of Eq. 4(a), the O–Ca–O angle, seems less important, since there are no significant differences among them in the different EPP optimized structures. Moreover its average and range are approximately the same as in the ideal structures, i.e., the square and tricapped trigonal prisms, used in the evaluation of the O–Ca–O angle when computing the average nonadditivity (see Sec. II A).

It is worth pointing out that specific nonadditive terms are neglected and might be one of the sources of the observed discrepancies. For instance, an interesting comparison can be made among structures III, VI, and VII. All of them have substantially the same first coordination shell (square antiprism). The presence of the ninth farthest water in structures VI and VII increases the differences between the RHF and EPP interaction energies with respect to the case of structure III.

We also notice how $\Delta E^{ab\ initio}$ for clusters with the same number of waters span a larger range than the corresponding ΔE^{EPP}. Instead, the energy separation between clusters with eight and nine waters are overestimated on average by EPP calculations, as a direct consequence of the larger discrepancies found for clusters with nine waters. Both facts should be connected just to the nature of the effective pair potentials that include implicitly many-body effects.

B. Calcium–ammonia clusters

In the case of ammonia clusters, the agreement between the *ab initio* and EPP results is even better, as can be observed from results shown in Fig. 4(b). As in the previous water case, minima with all molecules directly coordinating the ion were found for all the clusters at both levels. In particular, for $n=8$, different arrangements of ammonia molecules have also been investigated at EPP level. Only one minimum, corresponding to a $[Ca(NH_3)_8]^{2+}$ type of structure with a square antiprism arrangement, was found. Therefore, in this case, an octa-coordinated complex is clearly preferred.

However, when an additional ammonia molecule is considered, two different minima are obtained (structures I and II in Fig. 6). In structure I, the farthest molecule ($R_{\mathrm{Ca-N}}=4.44$ Å) is located in between the two square bases of the antiprism and interacts, via hydrogen bonds, with three ammonia molecules defining one of the triangular faces of the antiprism. In the case of structure II, the base structure of the square antiprism is maintained and the ninth one ($R_{\mathrm{Ca-N}}=3.76$ Å) is found along the S_8 axis of the antiprism.

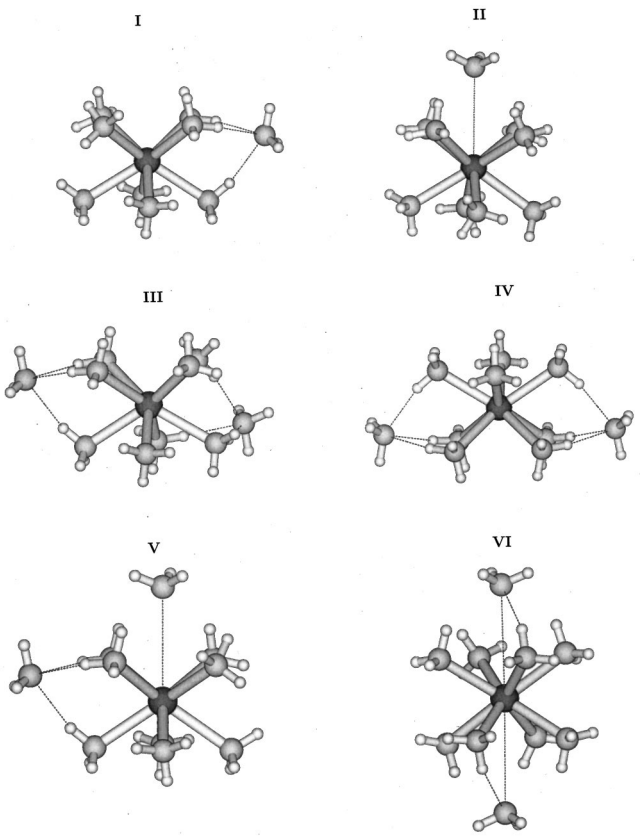

FIG. 6. Minima obtained for ammonia clusters containing nine and ten solvent molecules. The corresponding interaction energies are shown in Table IV. Atom coordinates are available as electronic data files (Ref. 62).

Helped by the increase of the N–Ca–N angles defined by the ammonia molecules belonging to the closest face, the ninth ammonia is in an intermediate situation between the first and the second coordination shells, while in structure I it is clearly in the second shell. The energies of both structures differ only by 0.3 kcal/mol, the situation with the most external molecule in the second shell being more stable. This can be considered as an analogous situation to that found for the water clusters with $n=8$, but now with nine ammonia molecules instead.

Finally, clusters with ten ammonia molecules have been explored. As in the previous case ($n=9$), all minima found contain eight molecules in the first shell. Four representative structures were identified corresponding to the possible combinations of the two minima found in the case of $n=9$ for the farthest molecule (structures III–VI in Fig. 6). In all cases, slightly distorted square antiprisms serve as base structures. Table IV shows the small range (<1 kcal/mol) of energies defined by the four structures.

From these results it can be inferred that a number of eight ammonia molecules in the closest neighborhood of the ion seems to be the most probable situation. However, outer ammonia molecules can be located in intermediate situations between the first two coordination shells, making feasible, at room temperature, easy distortions of the base structure (square antiprism) and, therefore, the possibility of transient situations in which two ammonia molecules interchange their

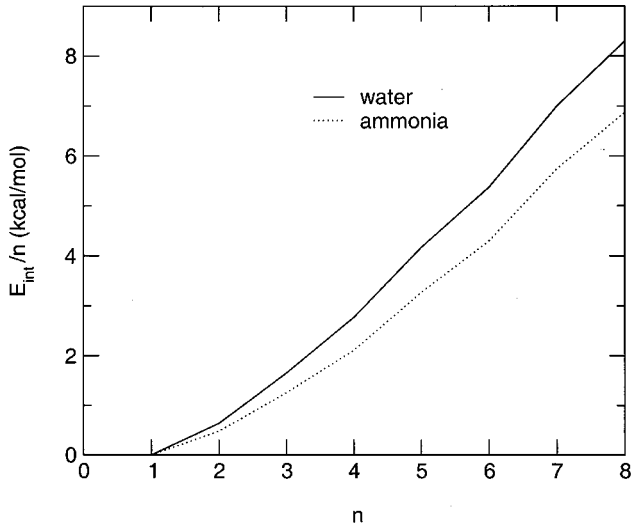

FIG. 7. Solvent–solvent interaction energy normalized to n as a function of the cluster size using the effective pair potentials. Structures used are those employed in Fig. 4.

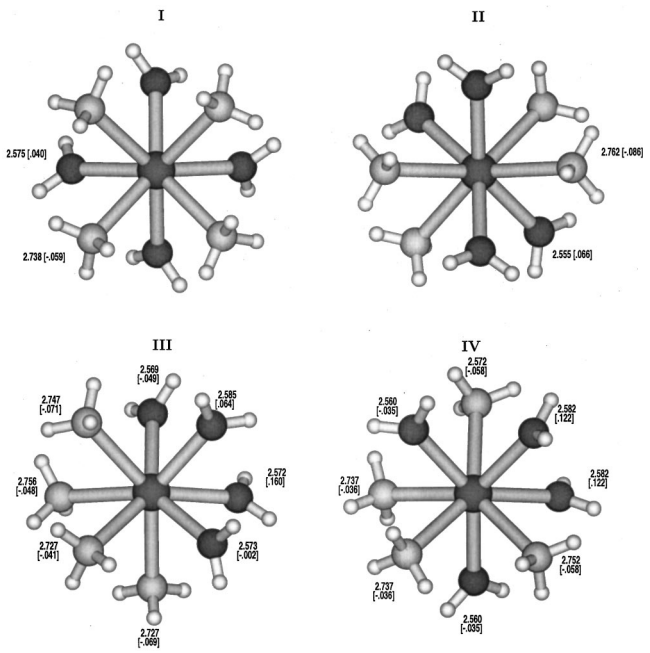

FIG. 8. Final EPP $[Ca(H_2O)_4(NH_3)_4]^{2+}$ geometries showing metal–ligand distances (R_{EPP}). Values in brackets correspond to the difference between the optimized *ab initio* distances ($R_{ab\ initio}$) in the cluster and the EPP ones ($R_{ab\ initio}-R_{EPP}$).

relative positions. This fact has been confirmed by short $[Ca(NH_3)_9]^{2+}$ cluster simulations at room temperature.

In any case, compared to the water case, results show how calcium ion is able to accommodate a larger number of ammonia molecules directly interacting with it. Because, as previously indicated, ion–water and ion–ammonia effective potentials are very similar in magnitude, $L-L$ interactions must play an important role with regard to the different observed behavior for the two ligands. First, the larger ion–N equilibrium distances in ammonia clusters reduces the repulsive ammonia–ammonia interactions present in the first coordination sphere. This fact can be observed in Fig. 7 where the water–water and ammonia–ammonia interaction energies as a function of the cluster size ($n=1-8$) are shown. Differences between both types of ligands continuously increase with the cluster size, water–water interactions always being more repulsive.

Second, while water is a good donor and acceptor of hydrogen bonds, ammonia is a much poorer donor, as has been shown by means of quantum chemical computations.[59] Interaction energies for the $(H_2O)_2$ and $(NH_3)_2$ optimized dimers, employing the SPC/E and OPLS potentials, follow this pattern as well. Therefore, the $L-L$ interaction between molecules in the first and second coordination shells acts in the same direction as the repulsive interaction between molecules in the first shell, both favoring a larger coordination number in calcium–ammonia clusters.

As for calcium–water clusters, the comparison between *ab initio* and EPP interaction energies on EPP optimized calcium–ammonia clusters shows that the use of EPPs slightly underestimates nonadditivity effects. Errors (2.4%–9%) are smaller than those found in calcium–water clusters and increase with the number of molecules.

Average Ca–N distance for ammonia in the first coordination shell is almost constant in all clusters shown in Fig. 6: 2.73–2.74 Å. This constancy must be attributed to the fact that in all cases the same basic polyhedrum defining the first coordination shell is found. Surprisingly, despite the difference between this value and that fixed in the representative geometry used to fulfill Eq. 4(c) (Ca–N=2.5 Å), performance of the Ca–NH_3 EPP is remarkable. To this end, the behavior of the calcium–ammonia clusters is rather different from that observed in the water case, where a correlation between ($\Delta E^{ab\ initio}-\Delta E^{EPP}$) and Ca–O average distances was found. Because of that constancy in the geometrical definition of the first coordination shell, the different errors obtained when comparing EPP and RHF interaction energies must be correlated with the specific n-body effects introduced by the ninth and tenth ammonia molecules.

C. $[Ca(H_2O)_4(NH_3)_4]^{2+}$ clusters

Symmetry properties, when present, reduce the number of initial structures resulting from the distribution of nL and mL' ligands in the $n+m$ positions of a selected polyhedron. For a square antiprism with $n=m=4$, this number is eight. The results presented here refer to a subset of four structures. Whatever of these selected structures clearly show the main effects of many-body interactions involving both ligands. In this case, structures were optimized at RHF and EPP levels. Figure 8 shows the final structures together with the metal–ligand distances for both types of calculations.

For clarity reasons, hereafter we will refer to a square antiprism as an ideal structure to discuss the geometrical and energetic results of these octa-coordinated mixed clusters. Using Scheme 1, N and/or O atoms of Fig. 8 can be identified with the A–H positions. In this framework, ''A'' and ''B'' define positions for closest neighbors, and ''A'' and ''E'' second closest neighbors. Overall, there are eight pairs of each kind.

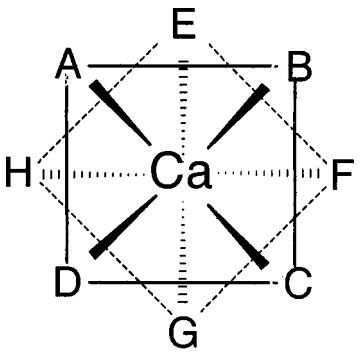

Scheme 1. Ligand distribution, and labeling, around calcium ion in an ideal square antiprism polyhedrum. Positions $a-b-c-d$ define the upper square base, and $e-f-g-h$ the bottom one.

A slight elongation of the Ca–O distances together with a slight shortening of the Ca–N distances are generally observed when *ab initio* structures are compared with the corresponding EPP ones. Differences are on average ~2%. Interestingly, these trends are opposite to those previously observed in the analysis performed for the $[Ca(H_2O)_8]^{2+}$ and $[Ca(NH_3)_8]^{2+}$ clusters (Fig. 4). We also notice that average Ca–O and Ca–N distances of EPP optimized $[Ca(H_2O)_4(NH_3)_4]^{2+}$ clusters are substantially the same as those found in $[Ca(H_2O)_8]^{2+}$ and $[Ca(NH_3)_8]^{2+}$ clusters, respectively. The slight differences, between both types of calculations, on the average distances in clusters of mixed composition is then a specific many-body effect of water–calcium–ammonia interactions.

In structures I and II, because of the symmetry present in the systems, the same metal–ligand distance is found for the four ligands of the same type. Comparing the final RHF and EPP metal–ligand distances, structure II presents a slightly larger effect on the Ca–O elongation and Ca–N shortening. This can be ascribed to the higher number (8) of three-body water–calcium–ammonia interactions involving the closest neighbors (N and O on the same ''square'' with $\angle$O–Ca–N$\simeq$74°). In structure I, where there are only three-body water–Ca–water and ammonia–Ca–ammonia interactions among the closest neighbors, three-body water–Ca–ammonia interactions involve all eight second closest neighbors (N and O on different ''squares faces'' with $\angle$O–Ca–N$\simeq$77°). This explains how the effect is significant also in structure I.

The symmetry breaking in structures III and IV is reflected in the Ca–O and Ca–N distances that now depend on the relative position occupied by the water/ammonia molecule. In both structures oxygens are involved in the same kind of interactions regarding the closest neighbors, while differences appear with regard to interactions with the second closest ones.

Precisely, in structure IV, the two farthest oxygens from calcium (positions ''B'' and ''F'' following Scheme 1) are involved in water–Ca–ammonia and water–Ca–water three-body interactions with the second closest neighbors. Instead, only the latter concern the oxygens with the shortest Ca–O distances (positions ''A'' and ''G''). The same kind of three-body interactions involving second neighbors are present in structure III, but with an opposite distribution with respect to the oxygens with farthest and shortest Ca–O distances. Therefore three-body interactions involving second neighbors cannot explain the differences observed in Ca–O distances. Therefore, this effect, likely a steric effect, has its origin in n-body interactions with $n>3$.

As subsequent analysis level, one can examine four-body subsystems containing the cation and three ligands. One finds that structures III and IV share four-body interactions involving calcium, one ammonia, and two waters. In this four-body subsystem there are the three-body interactions between closest and second neighbors ligands, in agreement with that noted previously. Therefore this four-body subsystem summarizes the analysis of three-body interactions made before.

A distinction between oxygens with shortest and longest Ca–O distances in both structures is finally found if five-body subsystems are identified. That referring to the two oxygens with the longest Ca–O distance also contains the calcium ion and two nitrogen atoms, those whose projections on the squares are connected to oxygens by diagonals. For clarity, in scheme 1, if the two O are located on positions ''B'' and ''F,'' the two N are on positions ''D'' and ''H''. The rest of the ligands plus the ion define the other five-body subsystem containing the two O with the shortest Ca–O distance and the other two N atoms. Projections on squares of O and N are again along square diagonals, but now there are also N–O pairs as second closest neighbors. Looking at Scheme 1, a N–O pair refers to positions ''A'' and ''C'' and the other to positions ''E'' and ''G.'' Likely, the interaction between the two five-body subsystems yields the final cluster geometries.

The effect of these small geometrical differences between the clusters optimized at EPP and RHF levels on the *ab initio* interaction energies (second column of Table IV) is, although small, non-negligible. For the mixed clusters, the situation is in between those found for the $[Ca(H_2O)_8]^{2+}$ and $[Ca(NH_3)_8]^{2+}$ clusters. In fact, EPP interaction energies are in very good agreement (2%–2.5%) with the *ab initio* calculation (see Table IV).

As for calcium–water and calcium–ammonia clusters, differences in ΔE are originated partially from differences in the optimized structures. Also in these clusters there is a compensation of errors, since the latter increase up to 5% when the comparison is made on the same structure (see Table IV). Finally, we notice that cluster interaction energy in octacoordinated complexes favors the substitution of water by ammonia in both kinds of calculation made on EPP optimized structures. Instead the substitution of ammonia by water is favored in RHF calculations if *ab initio* optimized structures are considered. These results do not invalidate the performance of the EPP potentials here presented. On the one hand, these have been built to describe effective interactions in liquid state, while RHF *ab initio* optimized structures refer to clusters *in vacuo*. On the other hand, favored geometries in the condensed phase might not be the same as those found in cluster optimizations. Moreover, it is the free energy and not the interaction energy that is the magnitude defining the final cluster stabilization.

IV. CONCLUSIONS

PCM methodology, as a strategy to develop effective *ab initio* pair potentials, has been extended to deal with multicomponent solutions. Particularly, calcium–water and calcium–ammonia effective pair potentials have been developed to study systems in which one or both types of ligands are present in the closest ion environment. As the dielectric constant used in the PCM computations is that of water at 298.5 K, the obtained potentials are more appropriate for water/ammonia systems, water being the main component.

Optimized geometries of $[Ca(H_2O)_n]^{2+}$ and $[Ca(NH_3)_n]^{2+}$ $(n=1-8)$ clusters, with frozen water and ammonia internal degrees of freedom, have been obtained by RHF *ab initio* calculations and using the developed effective *ab initio* pair potentials. Interaction energies and average distances versus *n* show that differences between the two kinds of calculations continuously decrease as long as *n* increases. These results show that *ab initio* effective pair potentials based on PCM properly describe the situation of an ion completely surrounded by (ligand/solvent) molecules, as is the case of the condensed phase.

Tests have also been made on different EPP optimized structures with a high number of ligands: $[Ca(H_2O)_n]^{2+}$ $(n=8,9)$, $[Ca(NH_3)_n]^{2+}$ $(n=8,9,10)$, and $[Ca(H_2O)_4(NH_3)_4]^{2+}$. In these cases, the agreement between both methodologies is not as good as in the case of using the resulting optimized structures at each level. Nevertheless, errors made by EPPs are always acceptable: 4%–10.5% in $[Ca(H_2O)_n]^{2+}$ clusters, 2.4%–9% in $[Ca(NH_3)_n]^{2+}$ clusters and 5% in $[Ca(H_2O)_4(NH_3)_4]^{2+}$ clusters. Comparing clusters with the same number of ligands $(n=8)$, errors are larger in calcium–water than in calcium–ammonia clusters, $[Ca(H_2O)_4(NH_3)_4]^{2+}$ clusters falling in between.

Cluster computations provide structural interesting tendencies as well. In particular, although just based on energetic contributions, the performed cluster analysis suggests that a reasonable upper limit for the hydration number of Ca^{2+} is eight. However, the information supplied by this analysis cannot discern between a hexa-, hepta- or octacoordinated as the more probable situation. Even more, based on the small differences observed, all structures could be sampled in the condensed phase at room temperature. The substitution of waters by ammonia molecules in the first hydration shell favors the tendency to accommodate a larger number of molecules in the nearest neighborhood of the ion. Water–water and ammonia–ammonia interactions, at first and first–second coordination shell levels, are pointed out as a key point to understanding the observed differences.

Tendencies observed in small clusters must be checked by subsequent statistical simulations. Preferred coordinations in small clusters can differ from those of the condensed phase where structures with a larger number of molecules directly bonded to the ion can also be favored. Facts like pressure, thermal effects, and the competition among the different kinds of interactions (e.g., first–second versus second–third coordination shell interactions) can certainly alter the conditions for preferential hydrogen bonding between molecules in the first and second coordination shells. In any case, small cluster computations become a useful reference in the interpretation of results obtained in the condensed phase.

The strategy presented in this work allows the inclusion of a realistic environment around the metal ion in mixed solvent situations at a very low computational cost during the potential development. In this sense, the potential application to more complex systems, like biomolecules, is clear. The approach could be used in the development of metal ion interaction potentials for standard force fields where solvent effects can be of primary importance if the ion interacts maintaining its first hydration shell to a large extent, as for instance in phosphate–metal ion interactions in nucleic acid simulations.

ACKNOWLEDGMENT

J.M.M. thanks the Ministerio de Educación y Cultura (M.E.C.) of Spain for a postdoctoral fellowship.

[1] B. E. Conway, *Ionic Hydration and Biophysics* (Elsevier, Amsterdam, 1981).
[2] J. P. Hunt and H. L. Friedman, Prog. Inorg. Chem. **30**, 359 (1983).
[3] *Ion Solvation*, edited by Y. Marcus (Wiley, Chichester, 1986).
[4] *The Physics and Chemistry of Aqueous Ionic Solutions*, edited by M. C. Bellisent-Funel and G. W. Neilson, NATO ASI Series C Vol. 205 (Reidel, Dordrecht, 1987).
[5] Y. Marcus, Chem. Rev. **88**, 1475 (1988).
[6] M. Magini, G. Licheri, G. Paschina, G. Piccaluga, and G. Pinna, *X-Ray Diffraction of Ions in Aqueous Solutions: Hydration and Complex Formation* (CRC Press, Boca Raton, FL, 1988).
[7] *Structure and Dynamics of Solutions*, edited by H. Ohtaki and H. Yamatera (Elsevier, Amsterdam, 1992).
[8] H. Ohtaki and T. Radnai, Chem. Rev. **93**, 1157 (1993).
[9] S. F. Lincoln and A. E. Merbach, Adv. Inorg. Chem. **42**, 1 (1995).
[10] *The Chemistry of Aqua Ions*, edited by D. T. Richens (Wiley, Chichester, 1997).
[11] *Physical Chemistry of Electrolyte Solutions*, edited by J. M. Barthel, H. Krienke, and W. Kunz (Steinkopff, Darmstadt, 1998).
[12] L. Helm and A. E. Merbach, Coord. Chem. Rev. **187**, 151 (1999).
[13] J. Gao, *Reviews in Computational Chemistry* (VCH, New York, 1996), Vol. 7, Chap. 3.
[14] R. Carr and M. Parrinello, Phys. Rev. Lett. **55**, 2471 (1985).
[15] T. Kerdcharoen, K. R. Liedl, and B. M. Rode, Chem. Phys. **211**, 313 (1996).
[16] A. Tongraar, K. R. Liedl, and B. M. Rode, J. Phys. Chem. A **101**, 6299 (1997).
[17] A. Berces, T. Nukada, P. Margl, and T. Ziegler, J. Phys. Chem. A **103**, 9693 (1999).
[18] D. Marx, M. Sprik, and M. Parrinello, Chem. Phys. Lett. **273**, 360 (1997).
[19] A. Tongraar, K. R. Liedl, and B. M. Rode, J. Phys. Chem. A **102**, 10340 (1998).
[20] A. Tongraar, K. R. Liedl, and B. M. Rode, Chem. Phys. Lett. **286**, 56 (1998).
[21] A. Tongraar and B. M. Rode, J. Phys. Chem. A **103**, 8524 (1999).
[22] G. W. Marini, K. R. Liedl, and B. M. Rode, J. Phys. Chem. A **103**, 11387 (1999).
[23] L. M. Ramaniah, M. Bernasconi, and M. Parrinello, J. Chem. Phys. **111**, 1587 (1999).
[24] T. Kerdcharoen and B. M. Rode, J. Phys. Chem. A **104**, 7073 (2000).
[25] M. I. Lubin, E. J. Bylaska, and J. H. Weare, Chem. Phys. Lett. **322**, 447 (2000).
[26] M. P. Allen and D. J. Tildesley, *Computer Simulations of Liquids* (Oxford University Press, Oxford, 1987).
[27] N. J. Elrod and R. J. Saykally, Chem. Rev. **94**, 1975 (1994).
[28] F. M. Floris and A. Tani, *Molecular Dynamics. From Classical to Quantum Methods* (Elsevier, Amsterdam, 1999), Vol. 7, p. 363.
[29] R. R. Pappalardo and E. Sánchez Marcos, J. Phys. Chem. **97**, 4500 (1993).
[30] R. R. Pappalardo, J. M. Martínez, and E. Sánchez Marcos, J. Phys. Chem. **100**, 11748 (1996).

[31] X. Periole, D. Allouche, A. Ramírez-Solís, I. Ortega-Blake, J. P. Daudey, and Y. H. Sanejouand, J. Phys. Chem. B **102**, 8579 (1998).
[32] X. Periole, D. Allouche, J. P. Daudey, and Y. H. Sanejouand, J. Phys. Chem. B **101**, 5018 (1997).
[33] J. M. Martínez, R. R. Pappalardo, and E. Sánchez Marcos, J. Chem. Phys. **109**, 1445 (1998).
[34] J. M. Martínez, R. R. Pappalardo, and E. Sánchez Marcos, J. Am. Chem. Soc. **121**, 3175 (1999).
[35] F. M. Floris, M. Persico, A. Tani, and J. Tomasi, Chem. Phys. Lett. **199**, 518 (1992).
[36] F. M. Floris, M. Persico, A. Tani, and J. Tomasi, Chem. Phys. Lett. **227**, 126 (1994).
[37] F. M. Floris, M. Persico, A. Tani, and J. Tomasi, Chem. Phys. **195**, 207 (1995).
[38] S. Miertuš, E. Scrocco, and J. Tomasi, Chem. Phys. **117**, 117 (1981).
[39] J. Tomasi and M. Persico, Chem. Rev. **94**, 2027 (1994).
[40] M. Odelius, C. Ribhing, and J. Kowaleski, J. Chem. Phys. **103**, 1800 (1995).
[41] E. Guardia, G. Sesé, J. A. Padró, and S. G. Kalko, J. Solution Chem. **28**, 1113 (1999).
[42] J. J. R. Fraústo da Silva and R. J. P. Williams, *The Biological Chemistry of the Elements* (Oxford University Press, Oxford, 1996).
[43] W. Kaim and B. Schwederski, *Bioinorganic Chemistry* (Wiley, Chichester, 1994).
[44] F. M. Floris, J. M. Martínez, and J. Tomasi, J. Chem. Phys. **116**, 5460 (2002), following paper.
[45] C. Amovilli and B. Menucci, J. Phys. Chem. B **101**, 1051 (1997).
[46] S. Petrie and L. Radom, Int. J. Mass. Spectrom. **192**, 173 (1999).
[47] T. Kerdcharoen and S. Hannongbua, Chem. Phys. Lett. **310**, 333 (1999).
[48] M. Pavlov, P. E. M. Siegbahn, and M. Sandstrom, J. Phys. Chem. A **102**, 219 (1998).
[49] M. J. Frisch, G. W. Trucks, H. B. Schlegel *et al.*, GAUSSIAN 99, Development Version Revision A.10+ Gaussian, Inc., Pittsburgh, PA, 1998.
[50] E. Cancès, B. Mennucci, and J. Tomasi, J. Chem. Phys. **107**, 3032 (1997).
[51] B. Mennucci, E. Cancès, and J. Tomasi, J. Phys. Chem. B **101**, 10506 (1997).
[52] W. S. Benedict, H. Gailar, and E. K. Pleyer, J. Chem. Phys. **24**, 1139 (1956).
[53] W. S. Benedict and E. K. Pleyer, Can. J. Chem. **35**, 1235 (1957).
[54] H. J. C. Berendsen, J. R. Grigera, and T. P. Straatsma, J. Phys. Chem. **91**, 6269 (1987).
[55] R. C. Rizzo and W. L. Jorgensen, J. Am. Chem. Soc. **121**, 4827 (1999).
[56] W. Smith and T. W. Forrester; DL_POLY (2.12 version), CCLRC, Daresbury Laboratory, 1999.
[57] A. K. Katz, J. P. Glusker, S. A. Beebe, and C. W. Bock, J. Am. Chem. Soc. **118**, 5752 (1996).
[58] F. Jalilehvand, D. Spangberg, P. Lindqvist-Reis, K. Hermansson, I. Persson, and M. Sandstrom, J. Am. Chem. Soc. **123**, 431 (2001).
[59] J. Gao and T. F. George, J. Phys. Chem. **97**, 9241 (1993).
[60] P. J. Hay and W. R. Wadt, J. Chem. Phys. **82**, 299 (1985).
[61] I. Ortega-Blake, J. C. Barthelat, E. Costes-Puech, E. Oliveros, and J.-P. Daudey, J. Chem. Phys. **76**, 4130 (1982).
[62] See EPAPS Document No. E-JCPSA6-116-305213 for atomic coordinate files of structures in Figs. 5 and 6. This document may be retrieved via the EPAPS homepage (http://www.aip.org/pubservs/epaps.html) or from ftp.aip.org in the directory /epaps/. See the EPAPS homepage for more information.